Effect of Sb-doping on martensitic transformation and magnetocaloric effect in Mn-rich $Mn_{50}Ni_{40}Sn_{10-x}Sb_x$ ($x = 1$, 2, 3, and 4) alloys*

Ishfaq Ahmad Shah, Najam ul Hassan, Jun Liu(刘俊), Yuanyuan Gong(龚元元), Guizhou Xu(徐桂舟), and Feng Xu(徐锋)†

Jiangsu Key Laboratory of Advanced Micro & Nano Materials and Technology, School of Materials Science and Engineering, Nanjing University of Science and Technology, Nanjing 210094, *China*

(Received 20 September 2016; revised manuscript received 2 October 2016; published online 8 December 2016)

We investigate the influence of Sb-doping on the martensitic transformation and magnetocaloric effect in $Mn_{50}Ni_{40}Sn_{10-x}Sb_x$ ($x = 1$, 2, 3, and 4) alloys. All the prepared samples exhibit a B2-type structure with the space group $Fm3m$ at room temperature. The substitution of Sb increases the valence electron concentration and decreases the unit cell volume. As a result, the magnetostructural transformation shifts rapidly towards higher temperatures as x increases. The changes in magnetic entropy under different magnetic field variations are explored around this transformation. The isothermal magnetization curves exhibit typical metamagnetic behavior, indicating that the magnetostructural transformation can be induced by a magnetic field. The tunable martensitic transformation and magnetic entropy changes suggest that $Mn_{50}Ni_{40}Sn_{10-x}Sb_x$ alloys are attractive candidates for applications in solid-state refrigeration.

Keywords: Mn-rich Heusler alloys, martensitic transformation, magnetocaloric effect, magnetic entropy change

PACS: 75.30.Sg **DOI:** 10.1088/1674-1056/26/1/017501

1. Introduction

In recent decades, magnetic cooling refrigerators based on the magnetocaloric effect (MCE) have received considerable attention. Compared with the traditional gas compression for refrigeration, magnetic cooling offers advantages in terms of low cost, safety, size, low mechanical vibration, high cooling efficiency, and environmental friendliness.[1–4] The application of magnetic refrigeration is strongly dependent on the MCE of materials. The large MCE observed in coupled materials has led to the widespread investigation of compounds that exhibit a magnetic first-order transition, e.g., $LaFe_{13-x}Si_x$,[5] $MnFeP_{0.45}As_{0.55}$,[6] $Gd_5Si_{4-x}Ge_x$,[7] and especially Ni-Mn-based ferromagnetic shape memory alloys.[8,9]

Recent experimental and theoretical work demonstrates that the MCE in Ni-Mn-based magnetic shape memory alloys is related to the thermal and magnetic-field-induced magnetostructural transformation (MT), which can be tuned by changing the valence electron concentration (e/a). The MT and coupled MCE have been widely investigated in Ni-rich Ni-Mn-based Heusler alloys, such as $Ni_{50}Mn_{37}Sn_{13}$,[10] $Ni_{43}Co_7Mn_{39}Sn_{11}$,[11] $Ni_{50}Mn_{36.5}Sb_{13.5-x}B_x$,[12] $Ni_{44}Co_{5.2}Mn_{36.7}In_{14.1}$,[13] $Ni_{50-x}Cu_xMn_{31}Ga_{19}$,[14] and $Ni_{50-x}Co_xMn_{31+x}Al_{19-x}$.[15] The MT and MCE are also observed in high-Mn-content Mn_2NiX (X = In, Sn, and Ga) inverse Heusler alloys.[16–18] It is known that $Mn_{50}Ni_{40}In_{10}$ alloy undergoes an MT from ferromagnetic austenite to weak magnetic martensite during cooling, and Co-doping leads to an increase in the magnetization difference (ΔM) between the two phases.[17,18]

A similar transition is observed in $Mn_{50}Ni_{40}Sn_{10}$ alloy. The MT in $Mn_{50}Ni_{40}Sn_{10}$ alloy is very sensitive to the p-d hybridization, which can be influenced by atomic substitution, resulting in a tunable MCE.[19,20] Attempts have been made to tune the MT through the partial substitution of Ni by Cu or Co in $Mn_{50}Ni_{40}Sn_{10}$ alloys.[21,22] However, the influence of sp-elements like antimony (Sb) on the MT and magnetic properties of Mn-rich Mn_2NiSn inverse Heusler alloys has not yet been reported. In the current work, $Mn_{50}Ni_{40}Sn_{10-x}Sb_x$ ($x = 1$, 2, 3, and 4) alloys are prepared by arc-melting. The effects of Sb-substitution on the structure, magnetic phase transition, and MCE around the MT are investigated and discussed in detail. Our results reveal that the MCE and transition temperature of $Mn_{50}Ni_{40}Sn_{10-x}Sb_x$ alloys are strongly dependent on the Sb concentration, and demonstrates that Sb-doped Mn_2NiSn alloys are competent candidates for refrigeration applications.

*Project supported by the National Natural Science Foundation of China (Grant Nos. 51271093, 51571121, 11604148, and 51601092), the Fundamental Research Funds for the Central Universities, China (Grant Nos. 30920140111010, 30916011344, and 30916011345), Jiangsu Natural Science Foundation for Distinguished Young Scholars, China (Grant No. BK20140035), China Postdoctoral Science Foundation (Grant No. 2016M591851), the Natural Science Foundation of Jiangsu Province, China (Grant Nos. BK20160833 and BK20160829), Qing Lan Project, Six Talent Peaks Project in Jiangsu Province, China, and the Priority Academic Program Development of Jiangsu Higher Education Institutions, China.

†Corresponding author. E-mail: xufeng@njust.edu.cn

© 2017 Chinese Physical Society and IOP Publishing Ltd

2. Experimental details

A series of polycrystalline Mn-rich $Mn_{50}Ni_{40}Sn_{10-x}Sb_x$ ($x = 1$, 2, 3, and 4) alloys were prepared by arc-melting the appropriate amounts of high-purity Mn, Ni, Sn, and Sb (99.95 wt.% purity) in an argon atmosphere. The samples were re-melted three times to enhance their homogeneity. The resultant samples were then sealed in vacuum quartz tubes and annealed at 1073 K for three days before being quenched in cold water. The martensitic transformations in the $Mn_{50}Ni_{40}Sn_{10-x}Sb_x$ ($x = 1$, 2, 3, and 4) alloys were identified by differential scanning calorimetry (DSC) in the temperature range 150–350 K with a cooling and heating rate of 10 K/min. The crystal structure was investigated by x-ray powder diffraction (XRD) using Cu-K_α radiation at room temperature (RT). The target compositions were confirmed through x-ray energy dispersive spectrometry (EDS), and the results are presented in Table 1. The magnetic measurements were carried out on a physical property measurement system (PPMS).

3. Results and discussion

The RT XRD patterns of the Mn-rich $Mn_{50}Ni_{40}Sn_{10-x}Sb_x$ ($x = 1$, 2, 3, and 4) alloys are shown in Fig. 1. The presence of (220), (400), and (422) peaks indicates that the $Mn_{50}Ni_{40}Sn_{10-x}Sb_x$ ($x = 1$, 2, 3, and 4) alloys exhibit a Heusler-type B2 structure with the space group $Fm3m$ at RT. Using the XRD data, the lattice parameter a and unit cell volume were calculated (listed in Table 1). Because the atomic size of Sb ($r = 1.59$ Å) is smaller than that of Sn ($r = 1.63$ Å), both a and unit cell volume decrease with increasing Sb content.

Table 1. The measured compositions and structural parameters of $Mn_{50}Ni_{40}Sn_{10-x}Sb_x$ ($x = 1$, 2, 3, and 4) alloys.

x	Mn/at.%	Ni/at.%	Sn/at.%	Sb/at.%	a/Å	Unit cell volume/Å^3
1	50.82	39.06	9.20	0.92	5.998	215.784
2	51.10	38.78	8.10	2.02	5.997	215.676
3	50.72	39.41	6.82	3.05	5.993	215.245
4	50.21	39.82	6.04	3.93	5.990	214.922

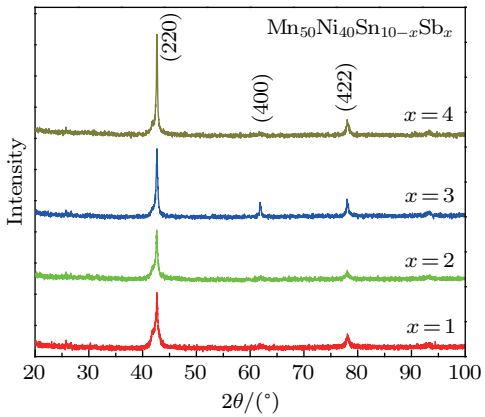


Fig. 1. (color online) XRD patterns of $Mn_{50}Ni_{40}Sn_{10-x}Sb_x$ ($x = 1$, 2, 3, and 4) alloys at room temperature.

The thermal-induced structural transformations in the $Mn_{50}Ni_{40}Sn_{10-x}Sb_x$ ($x = 1$, 2, 3, and 4) alloys were investigated by DSC in heating and cooling cycles. As shown in Fig. 2, large endothermic and exothermic peaks are observed, corresponding to the occurrence of the first-order structural transformation between martensite and austenite. As x increases from 1 to 4, the endothermic and exothermic peaks in the heating and cooling processes increase by 37 K and 38 K, respectively. It has been reported that the structural transformation temperature in Ni–Mn-based magnetic shape memory alloys is strongly related to e/a. The calculated e/a for the $Mn_{50}Ni_{40}Sn_{10-x}Sb_x$ ($x = 1$, 2, 3, and 4) alloys are given in Table 2. Here, the 3d and 4s electrons are considered as valence electrons in transition metals, and the 5s and 5p electrons are considered to be valence electrons in main-group elements. Because Sn has fewer 5p electrons than Sb, e/a increases with the Sb content. With the increase in e/a, the structural transformation shifts to higher temperatures. A similar relation between the structural transformation temperature and e/a has been observed in other Ni–Mn-based magnetic shape memory alloys.[22–25] Additionally, previous reports on Ge-doped NiMnSn and Ga-doped NiMnIn alloys indicate that the structural transformation temperature increases as the unit cell volume decreases.[26,27] In the present study, the Sb substitution causes the lattice to shrink, which may enhance the hybridization between Ni and Mn/Sn, leading to an increase in the structural transformation temperature.[28]

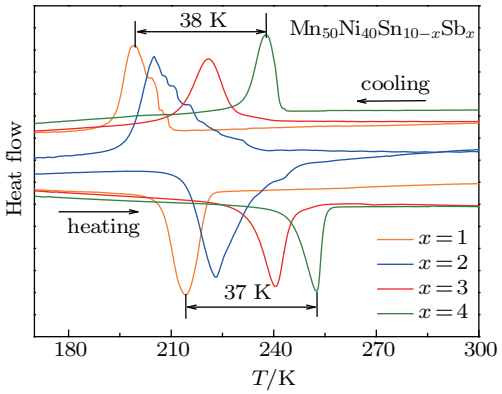


Fig. 2. (color online) DSC curves of $Mn_{50}Ni_{40}Sn_{10-x}Sb_x$ ($x = 1$, 2, 3, and 4) alloys.

Table 2. The martensitic start temperature (M_s), martensitic finish temperature (M_f), austenitic start temperature (A_s), austenitic finish temperature (A_f), and valence electron concentration (e/a) for $Mn_{50}Ni_{40}Sn_{10-x}Sb_x$ ($x = 1$, 2, 3, and 4) alloys.

x	M_s/K	M_f/K	A_s/K	A_f/K	e/a
1	207.8	193.4	206.8	220.7	7.877
2	215.8	197.6	213.8	230.8	7.882
3	228.3	212.1	232.3	243.9	7.916
4	242.1	230.9	244.9	254.1	7.935

Figure 3 shows the temperature dependence of magnetization ($M-T$) for the samples under an applied magnetic field

of 0.01 T in the heating and cooling processes. In the heating process, the $Mn_{50}Ni_{40}Sn_9Sb_1$ alloy experiences the magnetic order–disorder transition of martensite at approximately 170 K, followed by a sharp MT to ferromagnetic austenite at around 198 K. With further heating to 313 K, the magnetization in this sample gradually decreases to zero, corresponding to the Curie temperature of austenite. An obvious irreversibility between the heating and cooling curves is observed during the MT, indicating the first-order nature of this transition. The characteristic temperatures of the MT, austenitic start temperature A_s, austenitic finish temperature A_f, martensitic start temperature M_s, and martensitic finish temperature M_f, are listed in Table 2. As compared in Table 2 and Fig. 3, the MT shifts to higher temperatures as x increases, which agrees with the DSC measurements. As the transformation temperature is tuned to be close to the Curie temperature of austenite, the magnetization of austenite decreases remarkably with Sb substitution, leading to low values of ΔM.

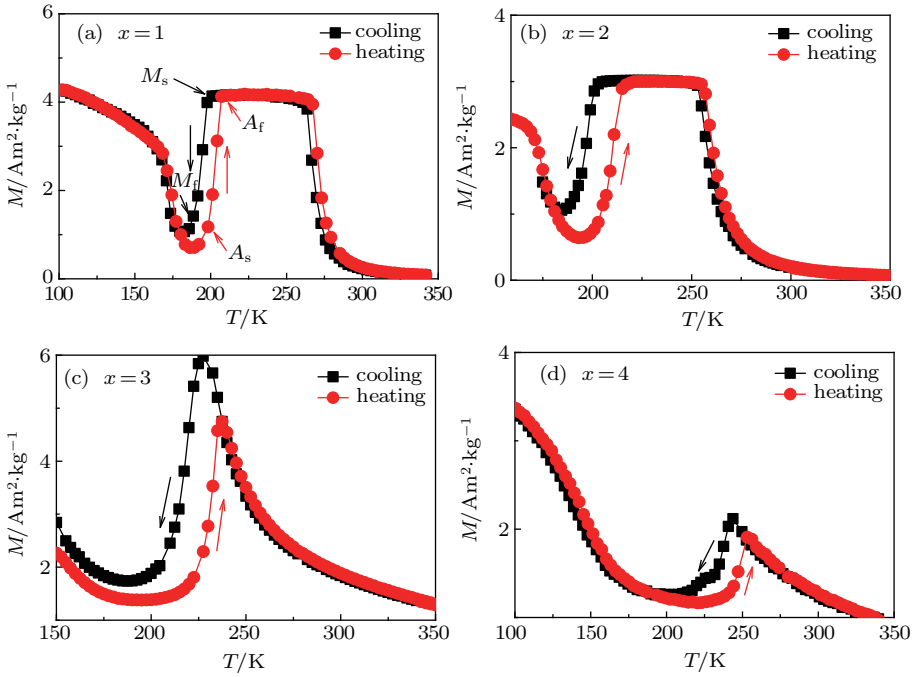


Fig. 3. (color online) $M-T$ curves for $Mn_{50}Ni_{40}Sn_{10-x}Sb_x$ alloys: (a) $x=1$, (b) $x=2$, (c) $x=3$, and (d) $x=4$, under an applied magnetic field of 0.01 T during the heating and cooling processes.

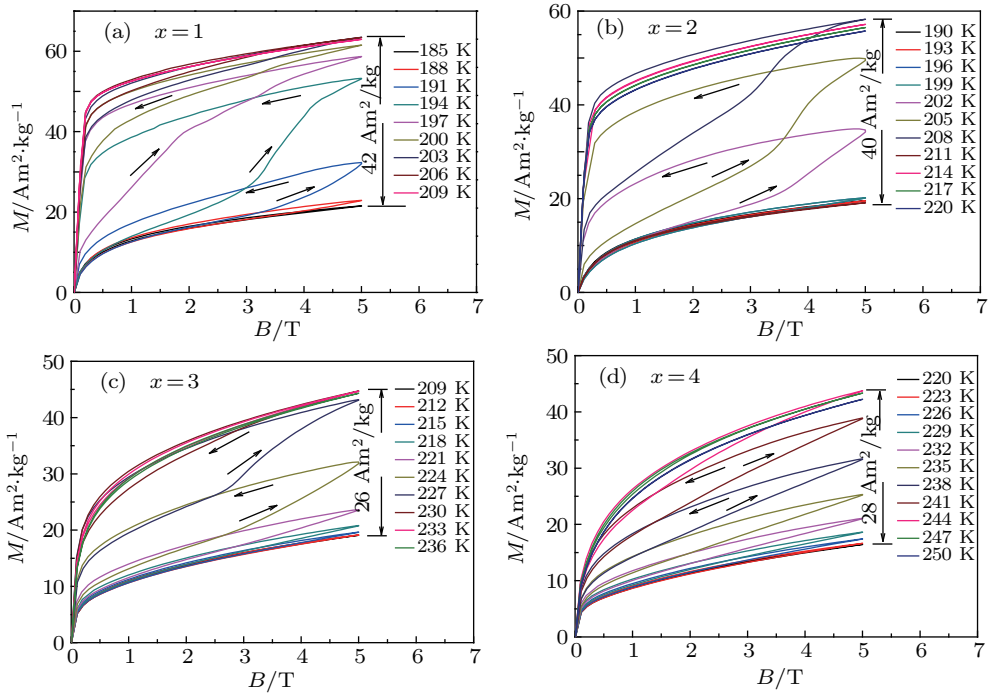


Fig. 4. (color online) M–B curves for $Mn_{50}Ni_{40}Sn_{10-x}Sb_x$ alloys: (a) $x=1$, (b) $x=2$, (c) $x=3$, and (d) $x=4$.

To study the magnetic properties around MT in more detail, the isothermal magnetization (M–B) was measured by the so-called loop method.[29] Before applying the magnetic field, the samples were cooled to full martensitic state, then slowly heated to the measurement temperature with a ramp rate of 3 K/min. As shown in Fig. 4, the metamagnetic behavior can be observed when the temperature is close to A_s, which corresponds to the magnetic field-induced MT from martensite to austenite. The existence of magnetic hysteresis indicates the first-order nature of the transition. The observed magnetic field-induced MT is related to ΔM between martensite and austenite.[30] For $x = 1$, 2, 3, and 4, the values of ΔM under 5 T are 42 A·m^2/kg, 40 A·m^2/kg, 26 A·m^2/kg, and 28 A·m^2/kg, respectively. The decrease of ΔM leads to the reduced magnetic field driving capacity in $Mn_{50}Ni_{40}Sn_6Sb_4$ alloy.

According to the M–B curves, the isothermal magnetic entropy change (ΔS_M) as a function of temperature was estimated under different magnetic field variations for $Mn_{50}Ni_{40}Sn_{10-x}Sb_x$ (x = 1, 2, 3, and 4) alloys using Maxwell's equation:[31]

$$\Delta S_{\mathrm{M}} = \int_0^B \left(\frac{\partial M(B,T)}{\partial T}\right)_B \mathrm{d}B. \quad (1)$$

As shown in Fig. 5, the maximum values of ΔS_{M} under a magnetic field variation of 0–5 T are 19.16 J·kg^{-1}·K^{-1}, 17.29 J·kg^{-1}·K^{-1}, 12.63 J·kg^{-1}·K^{-1}, and 8.65 J·kg^{-1}·K^{-1} for x = 1, 2, 3, and 4, respectively. As the magnetic field variation decreases to 0–2 T, the corresponding values reduce to 9.17 J·kg^{-1}·K^{-1}, 6.67 J·kg^{-1}·K^{-1}, 4.63 J·kg^{-1}·K^{-1}, and 2.88 J·kg^{-1}·K^{-1}, respectively. The values of ΔS_{M} decrease with the increase in Sb content. The maximum values of ΔS_{M} in Fig. 5 are comparable to those in $Mn_{50}Ni_{40-x}Co_xSn_{10}$ and $Ni_{50-x}Co_xMn_{32}Al_{18}$ ferromagnetic shape memory alloys.[32,33] As well as ΔS_{M}, the effective refrigeration capacity (RC_{eff}) is an important parameter for evaluating the magnetic cooling capacity of MCE materials. The RC_{eff} of $Mn_{50}Ni_{40}Sn_{10-x}Sb_x$ (x = 1, 2, 3, and 4) alloys was determined by subtracting the average hysteresis loss (HL) from the refrigeration capacity (RC). Here, the values of RC were obtained by integrating the area under the ΔS_{M} curves as a function of temperature within the full width at half maximum, and the average HL was calculated from the area surrounded by the M–B curves in Fig. 4. For $Mn_{50}Ni_{40}Sn_{10-x}Sb_x$ (x = 1, 2, 3, and 4) alloys, the RC values are found to be 131.9 J·kg^{-1}, 123.9 J·kg^{-1}, 72.1 J·kg^{-1}, and 71.9 J·kg^{-1} and the average HL values are 88.2 J·kg^{-1}, 84.8 J·kg^{-1}, 35.3 J·kg^{-1}, and 17.5 J·kg^{-1}, respectively. Therefore, the corresponding RC_{eff} is 43.8, 39.1 J·kg^{-1}, 36.8 J·kg^{-1}, and 54.5 J·kg^{-1} under a magnetic field variation of 0–5 T. Furthermore, as the MT of Mn-rich $Mn_{50}Ni_{40}Sn_{10-x}Sb_x$ alloys is highly dependent on the Sb content, the MCE can be tuned over a wide temperature range, which is a valuable property for magnetic refrigerants.

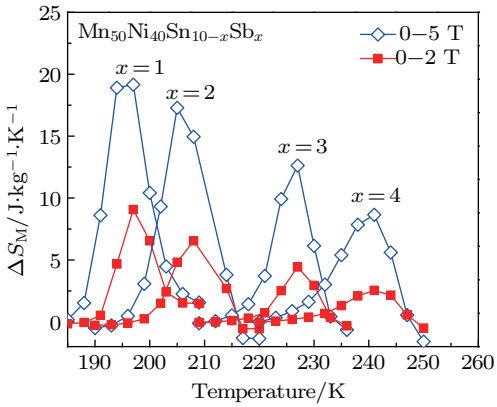


Fig. 5. (color online) Temperature dependent ΔS_M for $Mn_{50}Ni_{40}Sn_{10-x}Sb_x$ (x = 1, 2, 3, and 4) alloys.

4. Conclusion

In summary, we investigated the effect of Sb substitution on the martensitic transformation and magnetocaloric properties of $Mn_{50}Ni_{40}Sn_{10-x}Sb_x$ (x = 1, 2, 3, and 4) alloys. The Mn-rich $Mn_{50}Ni_{40}Sn_{10-x}Sb_x$ (x = 1, 2, 3, and 4) alloys have a B2-type structure at RT. As the Sb content increases, the MT shifts to higher temperatures. The magnetization difference between martensite and austenite means that the MT can be induced by an applied magnetic field. Obvious metamagnetic behavior can be observed in the M–B curves. The coupled maximum ΔS_M values with a magnetic field variation of 0–5 T are 19.16 J·kg^{-1}·K^{-1}, 17.29 J·kg^{-1}·K^{-1}, 12.63 J·kg^{-1}·K^{-1}, and 8.65 J·kg^{-1}·K^{-1} for x = 1, 2, 3, and 4, respectively. The tunable MCE indicates the potential for promising applications as a magnetic cooling refrigerant.

References

[1] Jaronie M J, Martin L, Aleksandar S and Mark A G 2014 *Mater. Design* **56** 1078
[2] Guillou F, Porcari G, Yibole H, Van Dijk N and Bruck E 2014 *Adv. Mater.* **26** 2671
[3] Gutfleisch O, Willard M A, Bruck E, Chen C H, Sankar S G and Liu J P 2011 *Adv. Mater.* **23** 821
[4] Zhang H and Shen B G 2015 *Chin. Phys. B* **24** 127504
[5] Hu F X, Shen B G, Sun J R, Wang G J and Cheng Z H 2002 *Appl. Phys. Lett.* **80** 826
[6] Tegus O, Bruck E, Buschow K and Boer F D 2002 *Nature* **415** 150
[7] Liu J, Gottschall T, Skokov K P, Moore J D and Gutfleisch O 2012 *Nat. Mater.* **11** 620
[8] Hu F X, Shen B G and Sun J R 2013 *Chin. Phys. B* **22** 037505
[9] Wang D H, Han Z.D, Xuan H C, Ma S C, Chen S Y, Zhang C L and Du Y W 2013 *Chin. Phys. B* **22** 077506
[10] Umetsu R Y, Sheikh A, Ito W, Ouladdiaf B, Ziebeck K R A, Kanomata T and Kainuma R 2011 *Appl. Phys. Lett.* **98** 042507
[11] Ma S C, Shih C W, Liu J, Yuan J H, Lee S Y, Lee Y I, Chang H W and Chang W C 2015 *Acta Mater.* **90** 292
[12] Luo H, Meng F, Jiang Q, Liu H, Liu E, Wu G and Wang Y 2010 *Scripta Mater.* **63** 569
[13] Gong Y Y, Wang D H, Cao Q Q, Liu E K, Liu J and Du Y W 2015 *Adv. Mater.* **27** 801
[14] Li P P, Wang J M and Jiang C B 2011 *Chin. Phys. B* **20** 028104

[15] Kainuma R, Ito W, Umetsu R Y, Oikawa K and Ishida K 2008 *Appl. Phys. Lett.* **93** 091906
[16] Tian L G, Hong L Z, Yan M F, Qiao M X and Heng W G 2013 *Chin. Phys. B* **22** 126201
[17] Llamazares J L S, Sanchez T, Santos J D, Perez M J, Sanchez M. L, Hernando B, Escoda L, Sunol J J and Varga R 2008 *Appl. Phys. Lett.* **92** 012513
[18] Wu Z, Liu Z, Yang H, Liu Y and Wu G 2011 *Appl. Phys. Lett.* **98** 061904
[19] Xuan H C, Zheng Y X, . Ma S C, Cao Q Q, Wang D H and Du Y W 2010 *J. Appl. Phys.* **108** 103920
[20] Liu Z H, Aksoy S and Acet M 2009 *J. Appl. Phys.* **105** 033913
[21] Xuan H C, Han P D, Wang D H and Du Y W 2014 *Intermetallics* **54** 120
[22] Hernando B, Llamazares J L S, Santos J D, Escoda L, Sunol J J, Varga R, Baldomir D and Serantes D 2008 *Appl. Phys. Lett.* **92** 042504
[23] Santos J D, Sanchez T, Alvarez P, Sanchez M L, Llamazares J L S, Hernando B, Escoda L, Suñol J J and Varga R 2008 *J. Appl. Phys.* **103** 07B326
[24] Han Z D, Wang D H, Zhang C L, Xuan H C, Gu B X and Du Y W 2007 *Appl. Phys. Lett.* **90** 042507
[25] Ito W, Xu X, Umetsu R Y, Kanomata T, Ishida K and Kainuma R 2010 *Appl. Phys. Lett.* **97** 242512
[26] Han Z D, Wang D H, Zhang C L, Xuan H C, Zhang J R, Gu B X and Du Y W 2009 *Mater. Sci. Eng. B* **157** 40
[27] Aksoy S, Krenke T, Acet M, Wassermann E F, Moya X, Manosa L and Planes A 2007 *Appl. Phys. Lett.* **91** 241916
[28] Priolkar K R, Lobo D N, Bhobe P A, Emura S and Nigam A K 2011 *Europhys. Lett.* **94** 38006
[29] Caron L, Ou Z Q, Nguyen T T, Thanh D T C, Tegus O and Bruck E 2009 *J. Magn. Magn. Mater.* **321** 3559
[30] Xuan H C, Han P D, Wang D H and Du Y W 2014 *J. Alloy. Compd.* **582** 369
[31] Han Z, Chen X, Zhang Y, Chen J, Qian B, Jiang X F, Wang D H and Du Y W 2012 *J. Alloys. Compd.* **515** 114
[32] Sharma J and Suresh K G 2015 *J. Alloys. Compd.* **620** 329
[33] Xuan H C, Chen F H, Han P D, Wang D H and Du Y W 2014 *Intermetallics* **47** 31